Received: June 16, 2020. Revised: July 13, 2020.

International Journal of
Intelligent Engineering & Systems

http://www.inass.org/

A New Local Gaussian Variational Level Set for Globus Pallidus Segmentation

Yohanes Setiawan[1] Chastine Fatichah[1] Riyanarto Sarno[1]*

[1]*Department of Informatics, Institut Teknologi Sepuluh Nopember, Indonesia*
* Corresponding author's Email: chastine@if.its.ac.id

Abstract: Globus Pallidus is an object in Magnetic Resonance Imaging (MRI) with severe intensity inhomogeneity and noises, such as small, low contrast, and weak boundary. Existing active contour methods fall into false boundaries while segmenting objects, which is smaller than the background like Globus Pallidus. This paper proposes a new local gaussian variational level set (NGVLS) for Globus Pallidus segmentation. We developed an energy term to create a smooth curve and prevent evolving curve into the false boundary. In the experiment, we compare NGVLS qualitatively and quantitively with existing methods such as Chan-Vese (CV), Region Scalable Fitting (RSF), Improved Region Scalable Fitting (Im-RSF), Local Pre-Fitting (LPF), and Local Gaussian Distribution Fitting (LGDF). We use Dice Similarity Coefficent (DSC) and Misclassification Error (ME) to measure the accuracy and error of the segmentation, respectively. The experiment is using 40 MRI datasets from Rumah Sakit National Hospital Surabaya, Indonesia. Qualitatively, the results show that NGVLS shows the best segmentation compared to the existing methods. Quantitatively, NGVLS achieves the highest average, minimum, and maximum value from DSC in 0.8291, 0.7119, and 0.9050, respectively. Also, NGVLS achieves the lowest average, minimum, and maximum value from ME in 0.0050, 0.0023, and 0.0155, respectively.

Keywords: New local gaussian variational level set, Globus pallidus, MRI, Segmentation.

1. Introduction

Neurodegenerative is a group of diseases that refers to the loss of progressive neuron cells without cause [1]. These diseases generally attack older people, e.g. Alzheimer and Parkinson's. Parkinson's Disease is known as the most common neurodegenerative disease after Alzheimer which is mostly affects older women [1], with symptoms such as shaking, stiffness, and balance, followed by several psychical disorders. However, diagnosing Parkinson's is difficult since it must recognize the patient's medical history and other diagnosis [2]. Therefore, we should use a diagnosis based on neurodegenerative disorder imaging to see the patient's brain structure.

Magnetic resonance imaging (MRI) is the most common neurodegenerative disorder imaging technology because of its good contrast quality, high resolution, and does not require any injection into the body [2]. Over the past three decades, MRI has been used to diagnose Parkinson's Disease and distinguish its type based on the patient's symptoms [3]. One of the techniques for diagnosing Parkinson's is to look at the structure of the Globus Pallidus, which is involved in electrical stimulation in the functional area of the inner brain structure of Parkinson's Disease [4]. Globus Pallidus is part of the subcortical brain or basal ganglia nuclei [5], whose structure is a small and low boundary in the brain. Consequently, the segmentation of Globus Pallidus in MRI is needed.

Image segmentation that divides image into several regions to separate the object from the background is rapidly developed. The segmentation process helps to group medical images to determine the desired anatomical objects [6] such as thick blood in microscopic images [7–9]. Globus Pallidus segmentation is also widely developed. Methods that have been developed using the brain atlas, or called atlas-based segmentation [5, 10], and based on deep learning [11]. The obstacle of the atlas-based method is making the atlas manually by experts which can take quite a long time. Meanwhile, the use of deep learning requires a large amount of training data that

is difficult to find. Besides that, deep learning computing is so high that a special computer is needed to execute the program.

Another segmentation method is Active Contour. Active Contour uses the concept of energy to carry out the process of contour evolution of its initial region of interest without the learning process Conventionally, Active Contour can be grouped into two models, namely edge-based and region-based [12]. Edge-based models or Snakes use edges in the image in for contour evolution such that very sensitive to noise [13]. Then, region-based model or Level Set guides the evolution of contours based on the inside and outside of the region with a region descriptor that significantly improves the edge-based model in handling objects with weak boundary [14]. Active Contour can be applied to medical images in very straightforward way, i.e. dental panoramic radiograph [15] and histophatological image [16]. One of the Active Contour with the popular Level Set model is the Chan-Vese Model (CV) [17]. CV developes energy functions related to Mumford-Shah segmentation, and the Level Set function was used to represent curves. However, CV uses global information and can not divide image regions that contain intensity inhomogeneity. Intensity inhomogeneity is a common problem that is caused by imperfections in the process of image acquisition, which causes variations in intensity in the same tissues [18]. Therefore, segmentation of images with intensity inhomogeneity is very difficult to do by methods that have assumption of uniform intensity [19]. The solution of the problem of intensity inhomogeneity in CV is proposed by [20], which is called Region-Scalable Fitting (RSF). RSF is able to deal with intensity inhomogeneity effectively through its evolutionary function, which can approximate the intensity locally in contour [20,21]. However, RSF is very dependent on the initial position of the the initial contour and not able to overcome images with severe intensity inhomogeneity. Next, [22] improves RSF with a new variational level set, namely Improved Region Scalable Fitting (Im-RSF). However, Im-RSF still can not handle severe intensity inhomogeneity as in RSF. After that, [14] develops Active Contour based on Local Pre-Fitting Function (LPF) with fast image segmentation. However, LPF cannot handle image with weak boundary and high noises. Then, [23] proposes Local Gaussian Distribution Fitting (LGDF) which is developed from bayes theory in the local gaussian distribution with mean and variance. LGDF considers local relationship to overcome intensity inhomogeneity with variational level set. It contains energy term as evolution driver, length and regularization term as smoother function and evolution stabilizer as used in RSF [20]. However, LGDF is hard to handle Globus Pallidus which has a smaller size than the background, since the energy term can spread the boundary into the background which reduces the cleanliness of segmentation result. Therefore, the false boundary is segmented.

In this research, we propose a new local gaussian variational level set (NGVLS) for the segmentation Globus Pallidus. NGVLS is developed from LGDF for contour evolution in local computation. NGVLS can smooth the curve into the boundary and avoid curve evolution to fall into false boundary in the range of initial contour. Firstly, we initialize the position of initial contour in Globus Pallidus manually. Secondly, we compute LGDF constants for the energy of the segmentation. Thirdly, we compute the gradient descent with NGVLS as our proposed method. Lastly, we update the contour until convergence and we get the Globus Pallidus segmentation. We compare NGVLS qualitatively and quantitively with existing methods such as Chan-Vese (CV) [17] , Region Scalable Fitting (RSF) [20], Improved Region Scalable Fitting (Im-RSF) [22], Local Pre-Fitting (LPF) [14], and Local Gaussian Distribution Fitting (LGDF) [23].

This organization of this paper is arranged as follows. Section 2 discusses the basic of existing Active Contour in image segmentation, especially medical images have problems in noise such as intensity inhomogeneity, weak boundary, and low contrast. Section 3 presents the materials and method for the segmentation of Globus Pallidus using our New Local Gaussian Variational Level Set. Section 4 describes the experiments and compares some existing methods with our proposed method. Finally, the conclusion and future work of this research are presented in Section 5. We give list of mathematical notations that is used in this paper in Table 1.

2. Literature review

Table 1. Mathematical notations

Notation	Denote
ϕ	Level set function
$*$	Convolution operator
$div(\dots)$	Divergence of vector
$\nabla\phi$	Gradient of level set function
$\nabla^2\phi$	Laplacian of level set function
$P(\phi)$	Distance regularization term
$\frac{\partial\phi}{\partial t}$	Implicit difference of level set function

2.1 Chan-vese model

The problem of edge-based models or Snakes that relies on image gradients to stop the curve evolution process results in the model only detect objects with edges that are defined by gradients, such that the curve is hard to detect boundary in noisy images [17]. Therefore, Chan-Vese (CV) model is not based on gradients in a stopping the process of curve evolution, but with the Mumford-Shah segmentation technique. The CV model can detect contours both with and without gradients as in objects with very smooth boundaries or non-continuous boundaries.

The CV model minimizes energy in the process of segmentation. Let curve C in image Ω as boundary C_0 of a region $\omega \subset \Omega$. Image u_0 is formed from inside region u_0^I and outside region u_0^O. CV fitting term with constant values c_1 and c_2 is given in Eq. (1).

$$F_1(C) + F_2(C) = \int_{u_0^I} |u_0(x,y) - c_1|^2 dxdy + \int_{u_0^O} |u_0(x,y) - c_2|^2 dxdy \quad (1)$$

CV model minimizes fitting term above and adds regularizing term $Length(C)$ and region area $Area(u_0^I)$ such that functional energy $F(c_1, c_2, C)$ can be defined in Eq. (2).

$$F(c_1, c_2, C) = \mu \ . \ Length(C) + v \ . \ Area(u_0^I) + \lambda_1 \int_{inside(C)} |u_0(x,y) - c_1|^2 dxdy + \lambda_2 \int_{outside(C)} |u_0(x,y) - c_2|^2 dxdy \quad (2)$$

Then, CV developing functional energy from Mumford-Shah with level set function ϕ for representing the curve as stopping process of curve evolution. The functional energy $F(c_1, c_2, \phi)$ is shown in Eq. (3).

$$\begin{aligned} &F(c_1, c_2, \phi) \\ &= \mu \, . \, Length(\phi = 0) + v . Area(\phi \geq 0) \\ &\quad + v \int_\Omega \delta\big(\phi(x,y)\big) |\nabla \phi(x,y)| \, dxdy \\ &\quad + \lambda_1 \int_\Omega |u_0 - c_1|^2 H\big(\phi(x,y)\big) \, dxdy \\ &+ \lambda_2 \int_\Omega |u_0(x,y) - c_2|^2 \Big(1 - H\big(\phi(x,y)\big)\Big) \, dxdy \end{aligned} \quad (3)$$

Where the definition of $Length(\phi)$, $Area(\phi)$, Heaviside function H_ϵ, and Dirac measure δ_ϵ is explained in Eqs. (4)-(7).

$$\begin{aligned} Length(\phi = 0) &= \int_\Omega |\nabla H_\epsilon(\phi)| \, dxdy \\ &= \int_\Omega \delta_\epsilon |\nabla \phi| \, dxdy \end{aligned} \quad (4)$$

$$Area(\phi \geq 0) = \int_\Omega |\nabla H_\epsilon(\phi)| \, dxdy \quad (5)$$

$$H_\epsilon(x) = \frac{1}{2}\left[1 + \frac{2}{\pi} \arctan\left(\frac{x}{\epsilon}\right)\right] \quad (6)$$

$$\delta_\epsilon(x) = H'_\epsilon(x) = \frac{1}{\pi}\left[\frac{\epsilon}{\epsilon^2 + x^2}\right] \quad (7)$$

Through the function above, the constant values c_1 and c_2 can be written in Eqs. (8) and (9).

$$c_1(\phi) = \frac{\int_\Omega u_0(x,y) H\big(\phi(x,y)\big) dxdy}{\int_\Omega H\big(\phi(x,y)\big) dxdy} \quad (8)$$

$$c_2(\phi) = \frac{\int_\Omega u_0(x,y) \big(1 - H\big(\phi(x,y)\big)\big) dxdy}{\int_\Omega \big(1 - H\big(\phi(x,y)\big)\big) dxdy} \quad (9)$$

The energy function is minimized to obtain changes in level set function ϕ with the partial differential equation as shown in Eq. (10). The computation of Eq. (10) is done by a numerical analysis approach using implicit finite differences.

$$\frac{\partial \phi}{\partial t} = \delta_\epsilon(\phi)[\mu \, div\left(\frac{\nabla \phi}{|\nabla \phi|}\right) - v - \lambda_1 (u_0 - c_1)^2 + \lambda_2 (u_0 - c_2)] \quad (10)$$

2.2 Region scalable fitting model

In CV model, image is assumed to have intensity homogeneity, which means the same object must have a homogeneous intensity [20]. This is certainly not suitable for the process of image segmentation with characteristic intensity inhomogeneity. When we applied the intensity homogeneity model to segment image with intensity inhomogeneity, the background can be detected as a region of interest.

In general, the case of images with intensity inhomogeneity often occur in medical images, which causes by technical problems or noises on the object being photographed. In MRI, intensity inhomogeneity is not generated by radio frequencies and the variation of object susceptibility. Therefore, the MRI segmentation process generally requires an enhancement process on the homogeneity of the intensity as a preprocess stage.

Region Scalable Fitting (RSF) model was proposed by [20] to overcome image with inhomogeneous intensity through region-based Active Contour. RSF is seen as a contour with two fitting functions which approximate the intensity of the image locally from the two sides of the contour. The optimal fitting function is the average of the local intensity of the two sides of the contour. The region-scalability is based on kernel functions with parameters that allows to use information from intensity in regions at controlled scales

Let $\Omega_1 = outside(C)$ and $\Omega_2 = inside(C)$. Energy function local intesity fitting ε_x^{Fit} is defined with Heaviside function $H(\phi)$ through $M_1 = H(\phi)$ and $M_2 = 1 - H(\phi)$ as shown in Eq. (11).

$$\varepsilon_x^{Fit}\big(\phi, f_1(x), f_2(x)\big) = \sum_{i=1}^{2} \lambda_i \int K_\sigma(x-y)|I(y) - f_i(x)|^2 M_i\big(\phi(y)\big)\, dy \tag{11}$$

In Eq. (11), $f_1(x), f_2(x)$ are two *fitting* values which approximates image intensity $\Omega_{i,} i = 1,2$, $I(y)$ is an intensy in local region which lies in the middle of coordinate y, and K_σ is Gaussian kernel as defined in Eq. (12).

$$K_\sigma(u) = \frac{1}{(2\pi)^{\frac{n}{2}}\sigma_n} \exp\left(-\frac{|u|^2}{2\sigma^2}\right) \tag{12}$$

The local intesity fitting ε_x^{Fit} is a weighted average square error from image intensity $I(y)$ from contour C by fitting value $f_1(x), f_2(x)$, with K_σ as weight which determines intensity $I(y)$ in pixel y. Then, the contribution of intensity $I(y)$ in energy function ε_x^{Fit} is reducing and approaching zero when the pixel y stays away from mid pixel x. Therefore, the energy ε_x^{Fit} is influenced by intensity $I(y)$ from pixel y inside neighborhood x.

RSF uses levet set regularization term in the level set function ϕ to maintain the regularization that needs for validation of computation and stabilization of level set curve. This level set regularization is defined in Eq. (13). After that, RSF minimizes energy function of contour evolution $F(\phi, f_1, f_2)$ as shown in Eq. (14).

$$P(\phi) = \int \frac{1}{2}(|\nabla\phi(x)| - 1)^2\, dx \tag{13}$$

$$F(\phi, f_1, f_2) = \varepsilon_x^{Fit}\big(\phi, f_1(x), f_2(x)\big) + \mu P(\phi) \tag{14}$$

In Eq. (14), μ is a positive constant. For minimizing the energy function, RSF uses gradient descent flow as the evolution curve equation. The function is computed through calculus of variation as show in Eq. (15).

$$f_i = \frac{K_{\sigma(x)} * [M_i(\phi(x) I(x)]}{K_{\sigma(x)} * M_i(\phi(x))}, i = 1,2 \tag{15}$$

Parameter f_1 and f_2 in Eq. (15) is fixed. Then, energy function F is minimized using the gradient flow equation as in Eq. (16), with e_1 and e_2 are function which includes Gaussian kernel as shown in Eq. (17).

$$\frac{\partial\phi}{\partial t} = \delta_\epsilon(\phi)\,(\lambda_1 e_1 - \lambda_2 e_2) + v\delta_\epsilon(\phi)\, div\left(\frac{\nabla\phi}{|\nabla\phi|}\right) + \mu\left(\nabla^2\phi - div\left(\frac{\nabla\phi}{|\nabla\phi|}\right)\right) \tag{17}$$

In Eq. (17), the first term is fitting data energy or data fitting term, which plays an important role for contour evolution. The second term is arc length term, which gives smoothing effects in zero level set contour Then, the third term is level set regularization which keeps regularization of level set function.

3. Materials and method

3.1 Local gaussian distribution fitting model

Image segmentation with Local Gaussian Distribution Fitting (LGDF) is developed using the distribution of local intensities through dividing image itu partitions from neighborhood [23]. Let Ω denotes an image domain for every point x. We defines a circular neighborhood $O_x \triangleq \{y \mid |x - y| \leq r\}$ with radius r. Then, $\{\Omega_i\}_{i=1}^n$ denotes a set of number of image regions n such that $\Omega = \bigcup_{i=1}^n \Omega_i$ and $\Omega_i \cap \Omega_j \neq \emptyset, \forall i \neq j$. The regions $\{\Omega_i\}_{i=1}^n$ is dividing image Ω based on the neighborhood O_x such that $\{\Omega_i\}_{i=1}^n = \{\Omega_i \cap O_x\}_{i=1}^n$. The segmentation of circular neighborhood O_x is considered as Max A Posteriori Probability (MAP).

Let $P(y \in \Omega_i \cap O_x | I(y))$ be the A Posteriori Probability of the subregions $\Omega_i \cap O_x$ with the neighborhood of intensity $I(y)$. Based on the Bayesian theorem, $P(y \in \Omega_i \cap O_x | I(y))$, or can be denoted by $P_{i,x}(I(y))$ is the probabilty density in region $\Omega_i \cap O_x$ with $P(y \in \Omega_i \cap O_x)$ as the A Priori Probability of Region $\Omega_i \cap O_x$ for all possible divided by neighborhood O_x and $P(I(y))$ as the A Priori Probability of Pixel Intensity $I(y)$. The Bayesian theorem is given in Eq. (18).

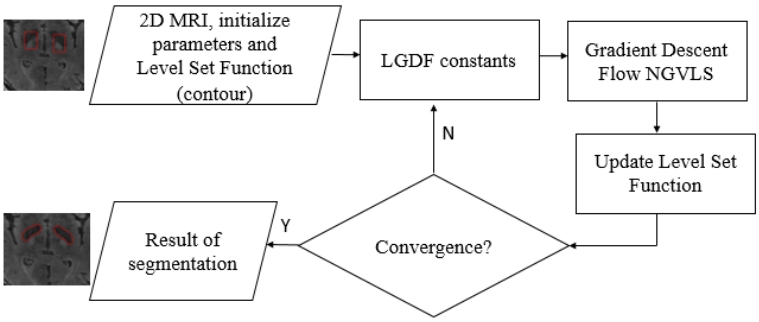

Figure. 1 Flowchart of the proposed method (NGVLS)

$$P\left(y \in \Omega_i \cap O_x \middle| I(y)\right) = \frac{P(y \in \Omega_i \cap O_x | I(y)\ P(y \in \Omega_i \cap O_x)}{P(I(y))} \quad (18)$$

Since the A Priori Probability Pixel Intensity $P(I(y))$ is independent of choosing regions and given all partitions are equally possible such that $P(y \in \Omega_i \cap O_x) = \frac{1}{n}$, therefore they can be neglected in computation of Bayesian theorem in this case. LGDF assumes the pixel for every region is independent such that the MAP can be achieved by the maximization of $P_{i,x}(I(y))$ across the regions O_x. Then, the maximization is converted to the minimization for getting energy of LGDF En_x^{LGDF} through taking a logarithm. The energy is defined in Eq. (17).

$$En_x^{LGDF} = \sum_{i=1}^{n} \int -\log |P_{i,x}(I(y))|\, dy \quad (19)$$

For approaching A Posteriori Probability $P_{i,x}(I(y))$, LGDF uses Gaussian probability density and assumes the mean and variance of the Gaussian distribution are spatially varying parameters. Therefore, the A Posteriori Probability $P_{i,x}(I(y))$ in Gaussian distribution with local average u_i and standard deviation σ_i can be written in Eq. (18).

$$P_{i,x}\left(I(y)\right) = \frac{1}{\sqrt{2\pi}\,\sigma_i} exp\left(\frac{\left(u_i - I(y)\right)^2}{2\sigma_i^2}\right) \quad (20)$$

Then, LGDF uses non-negative weighting function w for fast image segmentation such that object can be closer to be segmentated. The energy En_x^{LGDF} can be rewritten as in Eq. (21).

$$En_x^{LGDF} = \sum_{i=1}^{n} \int -w\ \log |P_{i,x}(I(y))|\, dy \quad (21)$$

In the case of image segmentation, the domain of image Ω can be divided into two regions: foreground (object) region Ω_F and background region Ω_B. There regions can be represented into level set functionϕ such that $\Omega_F = \{\phi < 0\}$ and $\Omega_B = \{\phi > 0\}$. Same with CV and RSF, LGDF uses $Length(\phi)$, $Area(\phi)$, Heaviside function H_ϵ, and Dirac measure δ_ϵ in the zero level set functions.

Parameters u_i and σ_i^2 in A Posteriori Probability $P_{i,x}(I(y))$ is minimized by calculus of variations such that satisfy Euler-Lagrange equations. Then, LGDF obtains u_i and σ_i^2 as given in Eqs. (22) and (23).

$$u_i = \frac{\int w\, I(y)\, M(\phi(y))dy}{\int w\, M(\phi(y))dy} \quad (22)$$

$$\sigma_i^2 = \frac{\int w\, \left(u_i - I(y)\right)^2\, M(\phi(y))dy}{\int w\, M(\phi(y))dy} \quad (23)$$

The funtional energy should be minimized through the solution of gradient descent flow equation as in RSF. The gradient descent flow includes energy term as the first term, length term as the second term, and regularization term that can be seen in Eq. (24). The constant e_1 and e_2 for driving LGDF segmentation is defined in Eqs. (25) and (26).

$$\frac{\partial \phi}{\partial t} = -\delta_\epsilon(\phi)\,(e_1 - e_2) + \nu\delta_\epsilon(\phi)\, div\left(\frac{\nabla\phi}{|\nabla\phi|}\right) + \mu\left(\nabla^2\phi - div\left(\frac{\nabla\phi}{|\nabla\phi|}\right)\right) \quad (24)$$

$$e_1 = \int w\left[\log(\sigma_1) + \frac{\left(u_i - I(y)\right)^2}{2\sigma_1^2}\right] dy \quad (25)$$

$$e_2 = \int w\left[\log(\sigma_2) + \frac{\left(u_i - I(y)\right)^2}{2\sigma_2^2}\right] dy \quad (26)$$

3.2 New local gaussian variational level set

We develop the energy term from LGDF by arctan variational level set [22] for limiting the segmentation range in image with severe intensity inhomogeneity. Consequently, the gradient descent flow is upgraded into the New Local Gaussian Variational Level Set (NGVLS) as in Eq. (27).

$$\frac{\partial \phi}{\partial t} = -\gamma\, \delta_\epsilon(\phi)\, arctan(e_1 - e_2) + \nu\, \delta_\epsilon(\phi)\, div\left(\frac{\nabla \phi}{|\nabla \phi|}\right) + \mu \left(\nabla^2 \phi - div\left(\frac{\nabla \phi}{|\nabla \phi|}\right)\right) \quad (27)$$

The $\arctan(...)$ function is used in NGVLS to manage and smooth the data driver. Parameter γ is a constant which sets the segmentation speed and limits the segmentation range such that the slope of the curve is fixed. This new gradient descent flow leads to as minimize as possible to the segmented image for having false boundary in the initialized contour.

The flowchart step of the proposed method of Globus Pallidus segmentation is shown in Fig. 1. The input is selected 2D MRI Image which concludes Globus Pallidus and then doing this following steps:

Step 1: Initialize the various parameters: number of iteration N, c_0, σ, Δt, γ, ν, μ, and zero level set function (contour) ϕ^0 in region of foreground Ω_F and region of background Ω_B in image Ω with pixel x as defined in Eq. (28).

$$\phi^0(x) = \begin{cases} -c_0, x \in \Omega_F \subset \Omega \\ c_0, x \in \Omega_B \subset \Omega \end{cases} \quad (28)$$

Step2: Compute LGDF constants e_1 and e_2 according to Eqs. (25) and (26)

Step3: Compute gradient descent flow NGVLS with Eq. (27)

Step4: Update the level set function evolution with Eq. (29)

$$\phi^{i+1}(x) = \phi^i(x) + \Delta t. \frac{\partial \phi}{\partial t} \quad (29)$$

Step5: Return to Step 2 until convergence or the maximum N is reached.

4. Results and analysis

4.1 Datasets

The MRI datasets are obtained from Rumah Sakit National Hospital in Surabaya, Indonesia. This research is using 40 MRI datasets which is from 40 patients.

The images are available in DICOM (.dcm) Format and in Sagittal slicing by default. Then, we change the default Sagittal slicing into Axial slicing for the need of seeing Globus Pallidus for the research. After that, we convert the DICOM into the BITMAP (.bmp) for 2D image segmentation using active contour and choose the image slice which contains Globus Pallidus. The ground truth images are segmented manually and confirmed by the experts (doctors).

4.2 Performance metrics evaluation

In this research, we measure the performance of segmentation result quantitatively. For the first performance metrics, we use Dice Similarity Coefficient (DSC) to calculate accuracy of the segmentation. Thus, the more DSC is close to 1, the more accurate the segmentation result.

Let S_M and S_G present region of segmentation from the model and ground truth, respectively. The segmentation from ground truth is achieved by manual segmentation which is must be confirmed by the experts. DSC is defined in Eq. (30).

$$DSC = \frac{2(S_M \cap S_G)}{S_M + S_G} \quad (30)$$

For the second performance metrics, we use Misclassification Error (ME) to measure the error of segmented foreground (object). As a result, the more ME is close to 0, the more minimize error of segmentation result produced by model from the ground truth.

Let F_G and B_G be the pixels of foreground and the background from the ground truth image, respectively. Let F_M and B_M be the pixels of foreground and the background from the model (segmented) image, respectively. ME is defined in Eq. (31).

$$ME = 1 - \frac{|F_G \cap F_M| + |B_G \cap B_M|}{|F_G| + |B_G|} \quad (31)$$

4.3 Comparison with existing methods

We compare NGVLS as the proposed method with popular existing methods such as Chan-Vese (CV) [17], Region Scalable Fitting (RSF) [20], Improved Region Scalable Fitting (Im-RSF) [22], Local Pre-Fitting (LPF) [14], and Local Gaussian Distribution Fitting (LGDF) [23]. The parameters of NGVLS are choosed by default for all images to test: $N = 200$, $c_0 = 1.0$, $\sigma = 5.0$, $\Delta t = 0.1$, $\gamma = 1.0$, $\nu = 0.001 \times 255 \times 255$, $\mu = 1.0$. We initialize the contour manually before segmentation on same position for every segmentation method before segmentation for comparing our proposed method with other existing methods.

We give examples result of experiment in Fig. 2 for qualitative analysis. As seen in Fig. 2 (a), Globus Pallidus as the object has smaller size than the background. CV, RSF, Im-RSF, and LPF have failed to segment Globus Pallidus very well. Performance

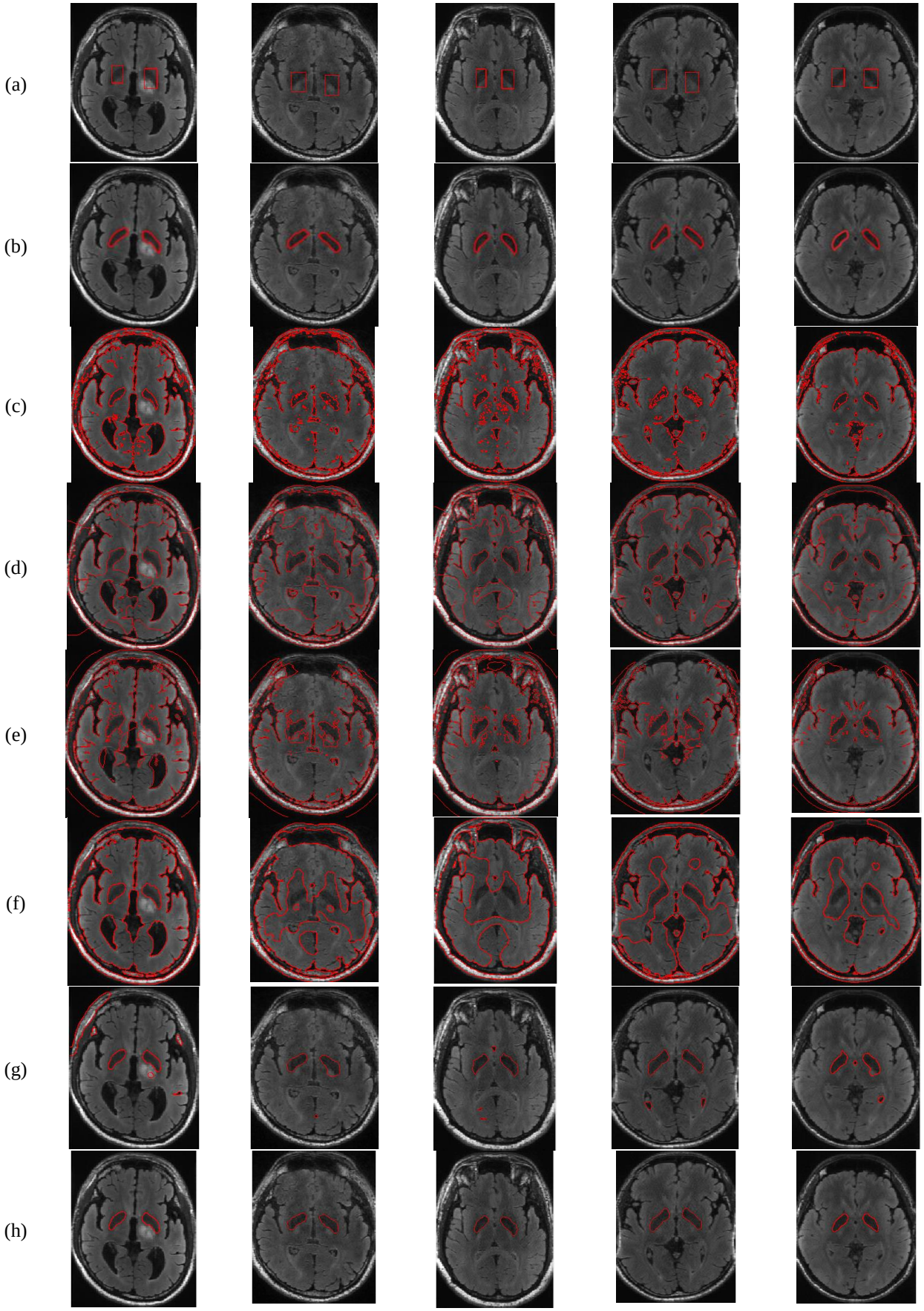

Figure. 2 Examples result of experiment: (a) initial contour, (b) ground truth, (c) result of CV [17], (d) result of RSF [20], (e) result of im-RSF [22], (f) result of LPF [14], (g) result of LGDF [23], and (h) result of NGVLS

Table 2. Comparison of performance metrics

Method	Evaluation Metrics	Descriptive Statistics			
		Average	Std	Min	Max
CV [17]	DSC	0.0216	0.0189	0.0015	0.0642
	ME	0.4659	0.0860	0.0052	0.5630
RSF [20]	DSC	0.0744	0.0239	0.0131	0.1199
	ME	0.2925	0.0741	0.1763	0.4923
Im-RSF [22]	DSC	0.0886	0.02682	0.0604	0.1937
	ME	0.2499	0.04650	0.1461	0.356
LPF [14]	DSC	0.0038	0.00330	0	0.011
	ME	0.3939	0.04958	0.1836	0.4692
LGDF [23]	DSC	0.6914	0.1730	0.276	0.8857
	ME	0.0129	0.0126	0.0024	0.0548
Proposed (NGVLS)	DSC	0.8291	0.0503	0.7119	0.905
	ME	0.005	0.0025	0.0023	0.0155

of CV depends on the edge quality of the image which assumes intensity homogeneity, while MRI has intensity inhomogeneity and the object Globus Pallidus is very low boundary and smaller than the background. RSF can not handle severe intensity inhomogeneity in the image such that the detected boundary is spread into background. Im-RSF is still can not handle severe intensity inhomogeneity as RSF. LPF can not handle weak boundary in Globus Pallidus such that it gives bad segmentation. LGDF shows better result since the local computation searches the object based on the initial contour. However, the result of segmentation is dirty. The background can be detected as object which effects on the cleanliness of the segmentation. Our proposed method (NGVLS) gives the best segmentation result. Through arctan variational level set, the contour is smooth through the boundary and the segmentation range is limited such that the curve is not fall into false boundary which improves LGDF in cleanliness of segmentation result.

The result of performance metrics is shown in Table 2. We give the comparison of performance metrics based on descriptive statistics for measuring the quantitative result of the experiments, such as average, standard deviation (Std), minimum value of the performance metrics (Min), and maximum value of the performance metrics (Max). As seen in Table 2, LPF performes the lowest value of DSC and the highest value of ME. This means the accuracy of segmentation is very little followed by the highest error in segmenting Globus Pallidus. Even though the Im-RSF achieves higher than CV and RSF, Im-RSF does not improve the accuracy and error of segmentation since CV, RSF, Im-RSF and LPF give small average DSC (below 0.1) and big ME (above 0.1). LGDF performes better than CV and RSF. However, LGDF still the biggest Std which means the spread of the segmentation result is variant. This can be seen that LGDF has very poor Min value and suddenly has very big Max value that means there is image with good segmentation and another with worst segmentation. Our proposed method (NGVLS) achieves the best segmentation result between existing methods with highest DSC in accuracy performance and lowest ME in error performance. Lower Std in NGVLS shows that each result is closer to the average. Then, the Min value of DSC is still high in 0.7119 and can achieve the Max value of DSC in 0.9050. The significance of NGVLS achieves the highest accuracy and the lowest error in segmenting Globus Pallidus is proved either qualitatively as in Fig. 2 or quantitatively as in Table 2.

5. Conclusion

This paper proposes a new local gaussian variational level set (NGVLS) for Globus Pallidus segmentation. NGVLS improves the energy term in LGDF with arctan function in case of smoothing contour into the boundary and avoiding segmented image into false boundary. NGVLS is evaluated quantitavely by looking the output image segmentation and qualitatively by calculating performance metrics, such as Dice Similarity Coefficent (DSC) for measuring accuracy and Misclassification Error (ME) for measuring error of segmentation. The performance metrics evaluation is presented by descriptive average, such as average, standard deviation (Std), minimum value of the performance metrics (Min), and maximum value of the performance metrics (Max).

The experiment is implemented on 40 MRI datasets which is converted into 2D images. The experimental results show that NGVLS achieves the best segmentation result both in quantitative and qualitative. Qualitatively, NGVLS is segmenting the Globus Pallidus accurately through the exact boundary. Quantitatively, NGVLS achieves the best

segmentation with the highest DSC average in 0.8291 and lowest ME average in 0.0050. The lower Std is proved the stabilization of each result from the average. Moreover, NGVLS is still achieve the highest result in Min (0.7119 in DSC and 0.0023 in ME) and Max (0.9050 in DSC and 0.0155 in ME).

Therefore, NGVLS as the proposed method gives significant improve to the segmentation of Globus Pallidus with characteristic of severe intensity inhomogeneity, low boundary, and having smaller size than the background. Furthermore, the segmentation of Globus Pallidus can be used for detecting Parkinson's Disease in medical application. For future work, NGVLS can be applied into other medical images for improving better image segmentation.

Conflicts of Interest

The authors have no conflict of interest

Author Contributions

As the first author, Yohanes Setiawan contributed to the formation of the paper, including the formulation of methods, the implementation of methods and the conduct of experiments. Chastine Fatichah assisted in formulation of the proposed method and checked the paper. Riyanarto Sarno supervised the preparation of the paper and proposes problem ideas that are handled in this paper.

Acknowledgments

The authors would like to sincerely thank Institut Teknologi Sepuluh Nopember, the Directorate of Higher Education, Indonesian Ministry of Education and Culture, and LPDP through RISPRO Invitation Program for funding the research.

References

[1] A. M. Al Radaideh and E. M. Rababah, "The role of magnetic resonance imaging in the diagnosis of Parkinson's disease: A review", *Clinical Imaging*, Vol. 40, pp. 987–996, 2016.

[2] O. Cigdem, I. Beheshti, and H. Demirel, "Effects of different covariates and contrasts on classification of Parkinson's disease using structural MRI", *Computers in Biology and Medicine*, Vol. 99, pp. 173–181, 2018

[3] B. Heim, F. Krismer, R. De Marzi, and K. Seppi, "Magnetic resonance imaging for the diagnosis of Parkinson's disease", *Journal of Neural Transmission*, Vol. 124, pp. 915–964, 2017.

[4] S. González Villà, A. Oliver, S. Valverde, L. Wang, R. Zwiggelaar, and X. Lladó, "A review on brain structures segmentation in magnetic resonance imaging", *Artificial Intelligence in Medicine*, Vol. 73, pp. 45–69, 2016.

[5] M. I. Iacono, N. Makris, L. Mainardi, J. Gale, A. Van Der Kouwe, A. Mareyam, J.R. Polimeni, L. L. Wald, B. Fischl, E. N. Eskandar, and G. Bonmassar, "Atlas-based segmentation for globus pallidus internus targeting on low-resolution MRI", In: *Proc. of International Conf. of the IEEE Engineering in Medicine and Biology Society*, pp. 5706–5709, 2011.

[6] I.N. Bankman, *Handbook of Medical Image Processing and Analysis*, Vol. 2, Academic Press, San Diego, S. D. 2008.

[7] U. Salamah, R. Sarno, A. Z. Arifin, Sarimuddin, A. S. Nugroho, I. E. Rozi, and P. B. S. Asih, "Segmentation of malaria parasite candidate from thickblood smear microscopic images using watershed and adaptive thresholding, Journal of Telecommunication", *Electronic and Computer Engineering*, Vol. 10, pp. 113–117, 2018.

[8] U. Salamah, R. Sarno, A. Z. Arifin, A. S. Nugroho, I. E. Rozi, and P. B. S. Asih, "Incorporating index of fuzziness and adaptive thresholding for image segmentation", *International Journal of Electrical and Computer Engineering*, Vol. 8, pp. 2406–2418, 2018.

[9] U. Salamah, R. Sarno, A. Z. Arifin, A. S. Nugroho, I. E. Rozi, and P. B. S. Asih, "A robust segmentation for malaria parasite detection of thick blood smear microscopic images", *International Journal on Advanced Science, Engineering and Information Technology*, Vol. 9, pp. 1450–1459, 2019.

[10] Y. Liu, Y. Wei, and C. Wang, "Subcortical Brain Segmentation Based on Atlas Registration and Linearized Kernel Sparse Representative Classifier", *IEEE Access*, Vol. 7, pp. 31547–31557, 2019.

[11] J. Dolz, C. Desrosiers, and I. Ben Ayed, "3D fully convolutional networks for subcortical segmentation in MRI: A large-scale study", *NeuroImage*, Vol. 170, pp. 456–470, 2018.

[12] X. Shan, X. Gong, and A. K. Nandi, "Active Contour Model Based on Local Intensity Fitting Energy for Image Segmentation and Bias Estimation", *IEEE Access*, Vol. 6, pp. 49817–49827, 2018.

[13] Y. Li, G. Cao, T. Wang, Q. Cui, and B. Wang, "A novel local region-based active contour model for image segmentation using Bayes theorem", *Information Sciences*, Vol. 506, pp. 443–456, 2020.

[14] K. Ding, L. Xiao, and G. Weng, "Active contours driven by local pre-fitting energy for fast image segmentation Active contours driven by local pre-fitting energy for fast image segmentation", *Pattern Recognition Letters*, Vol. 104, pp. 29–36, 2018.

[15] A. Z. Arifin, S. Adam, A. M. Mohammad, F. Anggris, R. Indraswari, and D. A. Navastara, "Detection of overlapping teeth on dental panoramic radiograph", *International Journal of Intelligent Engineering and Systems*, Vol. 12, No. 6, pp .71–80, 2019.

[16] N. S. Guptha and K. K. Patil, "Detection of macro and micro nodule using online region based-active contour model in histopathological liver cirrhosis", *International Journal of Intelligent Engineering and Systems*, Vol. 11, No. 2, pp. 256–265, 2018.

[17] T. F. Chan, L. A. Vese, "Active contours without edges", *IEEE Transactions on Image Processing*, Vol. 10, pp. 266–277, 2001.

[18] V. Uros, P. Franjo, and L. Bostjan, "A review of methods for correction of intensity inhomogeneity in MRI", *IEEE Transactions on Medical Imaging*, Vol. 26, pp. 405–421, 2007.

[19] K. Zhang, L. Zhang, K. M. Lam, and D. Zhang, "A Level Set Approach to Image Segmentation with Intensity Inhomogeneity", *IEEE Transactions on Cybernetics*, Vol. 46, pp. 546–557, 2016.

[20] C. Li, C. Y. Kao, J. C. Gore, Z. Ding, "Minimization of region-scalable fitting energy for image segmentation", *IEEE Transactions on Image Processing*, Vol. 17, pp. 1940–1949, 2008.

[21] C. Li, C. Y. Kao, J. C. Gore, and Z. Ding, "Implicit active contours driven by local binary fitting energy", In: *Proc. of the IEEE Computer Society Conf. on Computer Vision and Pattern Recognition*, 2007.

[22] B. Dong, R. Jin, and G. Weng, "Active contour model based on local bias field estimation for image segmentation", *Signal Processing: Image Communication*, Vol. 78, pp. 187–199, 2019.

[23] L. Wang, L. He, A. Mishra, and C. Li, "Active contours driven by local Gaussian distribution fitting energy", *Signal Processing*, Vol. 89, pp. 2435–2447, 2009.